International Journal of Thermal Sciences 184 (2023) 107970

Contents lists available at ScienceDirect

International Journal of Thermal Sciences

journal homepage: www.elsevier.com/locate/ijts

Numerical investigation of forced convection heat transfer from a sphere at low Prandtl numbers

I. Rodriguez [a,*], A. Campo [b]

[a] Turbulence and Aerodynamics Research Group (TUAREG), Universitat Politècnica de Catalunya (UPC), Colom 11, 08222, Terrassa(Barcelona), Spain
[b] 11110 Quail Rise, San Antonio, TX 78249, USA

ARTICLE INFO

Keywords:
Convective heat transfer
Sphere
Nusselt number
Low Prandtl number
Thermal wake

ABSTRACT

Direct numerical simulations of the flow and forced convective heat transfer around a sphere at Reynolds numbers between $Re = 500$ and $Re = 1000$ are performed. We investigate the effects of the Prandtl number (Pr) on the forced convective heat transfer from a sphere for various fluids having $Pr = 0.01, 0.1, 0.7$. At the larger Prandtl number, the convective transport due to the vortex shedding process dominates over the diffusive transport. As the Prandtl number decreases, diffusive effects become important. Moreover, the thermal boundary layer increases with decrements of the Prandtl number, which results in a reduction in the local and mean non-dimensional heat transfer coefficient. It is seen that at $Re = 500$ and $Re = 750$, the vortex shedding process is asymmetric, which results not only in a non-zero lift coefficient, but in an asymmetric temperature field in the wake of the sphere at $Pr \geq 0.1$. The dual asymmetry in the flow and the convective heat transfer is smooth out when the Prandtl number reaches $Pr = 0.01$ as the heat diffusion dominates and asymmetries in the vortex formation zone are no longer relevant in the heat transport. The descend in Prandtl number also produces an attenuation of the temperature fluctuations and thereby, in the turbulent heat transfer. As a direct consequence, two factors emerge at $Pr = 0.01$: (1) a lower decay ratio of the temperature in the wake centreline, and (2) a larger wake spread compared to higher Prandtl numbers.

1. Introduction

Forced and mixed convective heat transfer from spheres to fluids have been the topic focus of many research works for decades (e.g., [1–4]). Some of the most recent studies involving the fluid dynamics and heat transfer phenomena can be found in [5–10]. The particular case of forced convective heat transfer from spheres to low Prandtl number fluids, such as liquid metals is of interest in many engineering applications involving metallurgical processes, nuclear reactors, rocket fluid systems, among others. For instance, pebble-bed reactors (PBR), in which the pebbles (spheres) in the graphite-moderated nuclear reactor can be cooled with liquid sodium, instead of gas. Other specific applications can be the quenching of spherical metallic parts (like ball bearings) using helium-based binary mixtures instead of air [11]; the Prandtl number of these binary gas mixtures ranges between 0.1 and 1 [12].

Many theoretical, experimental and numerical studies have been documented in the literature in order to analyse the complex interweaving between fluid dynamics and heat transport, as well as to quantify the heat transfer rates from the spheres. One of the earlier theoretical works was performed by Hsu [13] who derived heat transfer correlations for spheres and elliptical rods exposed to liquid metals flows using assumptions of inviscid potential flow. With similar hypotheses, Sideman [14] also derived correlations for the Nusselt number in a sphere as a function of the Peclet number. Refai Ahmed and Yovanovich [15] proposed an analytical method based on the linearisation of the energy equation for obtaining a solution for the heat transfer from an isothermal sphere in the range of Reynolds numbers $0 \leq Re \leq 2 \times 10^4$ and all Prandtl numbers. A correlation for estimating the Nusselt number was also proposed. Although the predicted heat transfer was in good agreement with most of the results available in the literature, larger deviations were observed when comparing with results involving low Prandtl numbers. Another analytical solution to forced convection heat transfer from a sphere to low Prandtl numbers $Pr < 1$ in laminar regime was presented by Kendoush [16]. He derived correlations for the heat transfer rates at the front and rear stagnation points in the sphere, as well as for the local and overall Nusselt number. The agreement with results from the literature was reasonable, although these comparisons were done for $Pr = 0.7$ and the applicability to lower Prandtl number fluids was not tested.

Regarding experimental measurements of the heat transfer from a sphere, many studies have embarked on obtaining correlations for

* Corresponding author.
E-mail addresses: ivette.rodriguez@upc.edu (I. Rodriguez), campanto@yahoo.com (A. Campo).

https://doi.org/10.1016/j.ijthermalsci.2022.107970
Received 11 November 2021; Received in revised form 13 September 2022; Accepted 3 October 2022
Available online 17 October 2022

the Nusselt number, but also for the local heat transfer rates at the front and back stagnation points (see for instance [6,17–19]). Some of the experimental studies carried out also considered the effect of variable fluid properties on the estimation of the heat transfer [20–22]; however, most of the results were devoted at Prandtl number $Pr \geq 0.7$.

Among the experimental works involving low Prandtl numbers, the pioneering work of Witte [23] using liquid sodium can be mentioned. He measured the heat transfer from spheres in the range of Reynolds numbers of $3.56 \times 10^4 < Re < 1.525 \times 10^5$. The results were compared to available correlated results for heat transfer in water and air, but sensible differences were observed. The Nusselt numbers measured were consistently lower of those for larger Prandtl number fluids. Argyropoulos and Mikrovas [24] also measured the heat transfer from spheres in liquid metals under natural and forced convection conditions and pertinent results were correlated for both conditions. The melting time of spheres exposed to different Prandtl numbers in the range of $0.001 < Pr < 10$ was later measured by Melissari and Argyropoulos [25]. Significant differences in terms of the buoyancy parameter, as well as on the ratio of the thermal to viscous boundary layers were observed depending on the Prandtl number.

From the platform of numerical calculations, the heat transfer from a sphere has also be examined in several investigations. Feng and Michaelides [26] presented a solution to the unsteady heat and mass transfer from an isothermal sphere in a viscous fluid at low Peclet numbers when its surface undergoes a step change in the temperature. Later, the authors performed a two-dimensional numerical study for Reynolds numbers up to $Re = 4000$ with Prandtl numbers in the range of $0.1 < Pr < 10$ [27]. They found a weak dependence of the heat transfer rate for $Pe < 2$, whereas for large Peclet numbers a strong dependence on the Reynolds number was observed. Dhole et al. [28] conducted a two-dimensional numerical study to analyse the thermal convection from an isothermal sphere in the combined ranges of Reynolds numbers $5 \leq Re \leq 200$ and Prandtl $0.7 \leq Pr \leq 400$. Based on the results obtained, a numerical correlation for the heat transfer coefficient was developed. Acceptable results were attested in comparison to other correlations reported in the literature.

More recently, the heat transfer characteristics of a variable property fluid and a sphere in the laminar Reynolds number range of $10^{-3} \leq Re \leq 10$ was studied by Ganguli and Lele [29]. The authors observed large deviations in the drag coefficient with increments in temperature. Aside from this, they proposed correlations for the drag and Nusselt number that adequately fit the numerical results in the range analysed.

The influence of Prandtl number on the transport characteristics for steady laminar mixed convection from a sphere was numerically studied by Raju et al. [8] employing Reynolds numbers in the range of $5 \leq Re \leq 200$, Richardson numbers $0 \leq Ri \leq 1.5$ and Prandtl numbers $0.7 \leq Pr \leq 40$. In their study, the variation of the Nusselt number susceptible to different conditions was analysed. Later, these authors also conducted studies for mixed convection heat transfer from a sphere with constant heat flux for liquid metals [30]. Different Reynolds numbers in the range of $5 \leq Re \leq 200$, Prandtl $0.02 \leq Pr \leq 0.06$ and Richardson numbers $0 \leq Ri \leq 5$ were considered. Although no larger differences were detected in the range of Prandtl numbers studied, it was demonstrated that when the Richardson number was expanded, the recirculation length diminished and eventually was suppressed for the larger Ri. Later, the authors extended the study to cover larger Prandtl numbers $0.7 \leq Pr \leq 20$ arriving at similar conclusions on the dependence of the recirculation region with the Richardson number [10].

So far, the plethora of studies regarding the influence of the Prandtl number on the heat transfer in a sphere/fluid ensemble has been focused on obtaining correlations for the Nusselt number, either by experiments or using simplified numerical methodologies, or in analysing the fluid dynamics and heat transfer in the wake at very low Reynolds numbers. In the context of engineering applications mentioned at the beginning of the introduction, to have a profound knowledge of the heat transfer is key if efficiency and productivity are considered. In such endeavours, the Prandtl number has an important bearing on the heat transfer and wake characteristics. Thereby, it is obvious that there is a need for gaining insight into the impact of Prandtl number in the range of Reynolds numbers in which the flow is unsteady and transitional to turbulence. Regrettably, few studies addressing this regime can be found in the literature. Among them, Rodriguez et al. [9] performed a numerical study in the turbulent regime, accounting for Reynolds numbers up to $Re = 10^4$, but restricted to a constant Prandtl number $Pr = 0.7$. Special emphasis was placed on the quantification of the heat transport from the sphere to the fluid along with the detailed characterisation of the thermal wake. More recently, the analysis was extended to incorporate the impact of the free-stream turbulence upon the heat transfer patterns [31]. In light of the foregoing observations, the present study focuses on the role of the Prandtl number on the fluid dynamics and heat transfer from a sphere and on the intricacies of the thermal wake. To accomplish this, direct numerical simulations for Reynolds numbers of $Re = 500$, 750 and 1000 (here U is the free-stream velocity and D is the sphere diameter) and Prandtl numbers in the range $Pr = 0.01 - 0.7$ are performed.

The work is organised as follows. In the next section the description of the mathematical and numerical models used, the computational domain and mesh assessment are given. In Section 3, a discussion of the effects of the Prandtl number on both instantaneous and average temperature field, as well as on the local and average non-dimensional heat transfer coefficients is presented. Moreover, the analysis of the thermal wake characteristics considering the effects on the heat transport is also presented. Final conclusions are drawn in Section 4.

2. Description of the mathematical model and the numerical method

In the present work, the relevance of the Prandtl number on the heat transfer ratio from a sphere is investigated. Different Reynolds numbers $Re = U\,D/\nu = 500$, 750 and 1000 and Prandtl numbers $Pr = \nu/\kappa = 0.01$, 0.1 and 0.7 are considered. The latter encompasses fluids ranging from liquid metals (such as sodium $Pr = 0.004 - 0.01$, gallium $Pr = 0.025$, lead–lithium $Pr = 0.01 - 0.04$) to air ($Pr = 0.71$) passing through binary gas mixtures (e.g., helium–xenon $Pr = 0.12$) [12,32,33]. The wake regimes span from the unsteady laminar regime to the onset of the turbulent regime [34,35].

The fluid dynamics and heat transfer from a sphere to a fluid is governed by the Navier–Stokes and energy equations. Assuming an incompressible viscous Newtonian fluid with constant thermo-physical properties and neglecting the effects of thermal radiation, the system of equations read

$$\frac{\partial u_i}{\partial x_i} = 0 \tag{1}$$

$$\frac{\partial u_i}{\partial t} + \frac{\partial u_i u_j}{\partial x_j} - \nu \frac{\partial^2 u_i}{\partial x_j \partial x_j} + \rho^{-1} \frac{\partial p}{\partial x_i} = 0 \tag{2}$$

$$\frac{\partial T}{\partial t} + \frac{\partial u_i T}{\partial x_j} - \kappa \frac{\partial^2 T}{\partial x_j \partial x_j} = 0 \tag{3}$$

where x_i represents the spatial coordinates with $i = 1, 2, 3$ (or x, y, and z); t is the time; u_i (or u, v, and w) denotes the velocity components in the three directions; p and T stand for the pressure and temperature fields, respectively. The participating fluid properties are the kinematic viscosity ν, density ρ and thermal diffusivity κ.

To solve the above system of equations, the code Alya has been used [36]. In the Alya platform, the equations are discretised using a low-dissipation finite element (FE) scheme [37] that preserves linear/angular momentum and kinetic energy at discrete levels. The scheme is implemented in equal order finite elements, which has been proven to be suitable for simulating turbulent flows. For the pressure–velocity coupling, a non-incremental fractional-step method is used to stabilise the pressure. For the time marching algorithm, the

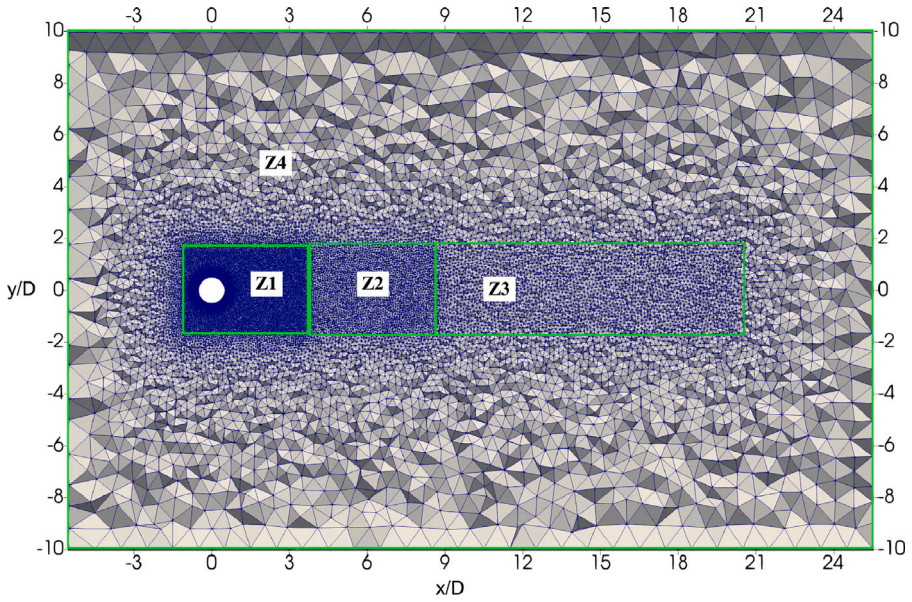

Fig. 1. Central plane of the computational domain, mesh m1 (see Table 1 for details of the sizes of the different zones).

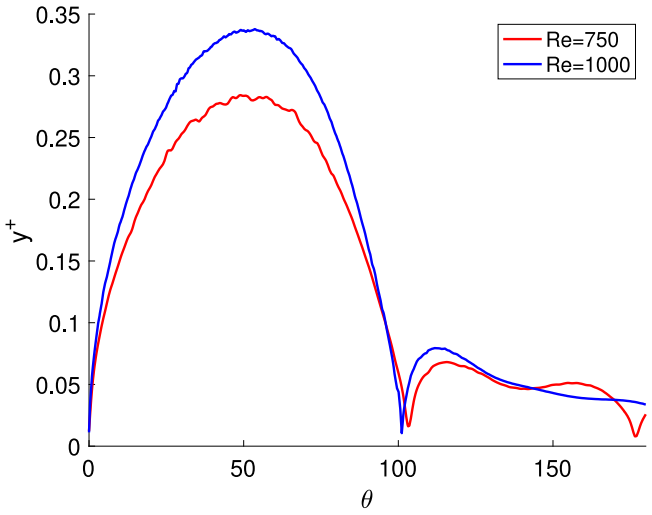

Fig. 2. Wall-normal distance y^+ along the sphere circumference for $Re = 750$ using mesh m1 and $Re = 1000$ using mesh m2.

system of equations is explicitly integrated using a fourth order Runge–Kutta method proposed by Capuano et al. [38] and combined with an eigenvalue-based time-step estimator [39], which allows dynamically adapt the time-step without losing accuracy (for more details, the reader is referred to Trias and Lehmkuhl [39]). The low-dissipation strategy implemented here was extensively tested for different turbulent flows in Lehmkuhl et al. [37]. Also, this strategy has been enforced for tackling a multitude of complex problems, such as the flow past a cylinder, fluid–structure interaction, impinging jets for cooling or active flow control of wings (see for instance [40–43]). Moreover, the methodology delineated here proved to yield accurate results in the context of the fluid dynamics and heat transfer from a sphere to non metallic fluids (see Rodríguez et al. [9,31]).

2.1. Computational domain and boundary conditions

The computational domain to be adopted has been utilised before as manifested in Refs. [9,31,44], i.e., a cylindrical domain of dimensions $(x, r, \theta) \equiv [(-5.5D : 25.5D); (0 : 10D); (0 : 2\pi)]$ with the sphere located at the origin $(0, 0, 0)$. In previous works, extensive comparisons with the literature values for the flow field (e.g., local pressure coefficient, velocity profiles in the wake, among other quantities) as well as heat transfer (e.g., heat transfer coefficient) were performed. Overall, the obtained results were in good agreement with the reported experimental and numerical results. Therefore, no further studies revolving around the influence of the computational domain and/or the numerical method are deemed necessary here.

As far as the boundary conditions is concerned, a uniform velocity profile $(u/U, v/U, w/U) = (1, 0, 0)$ and a constant temperature $\Theta = (T - T_{in})/(T_{sph} - T_{in}) = 0$ are imposed at the inlet. Here, the non-dimensional temperature Θ is defined in terms of the inlet temperature T_{in} and the sphere surface T_{sph}. Owing that in the forced convection heat transfer regime under study the velocity and temperature fields are uncoupled, the energy equation can be interpreted as the transport of a passive scalar and then, the actual values of the temperature at the inlet and at the sphere surface are irrelevant. With regards to the outlet, a pressure-based condition is imposed for the momentum equations. For more details, the reader is referred to Rodriguez et al. [9,44]. For the temperature, a Neumann boundary condition, i.e., $\partial\Theta/\partial n = 0$ (n being the normal direction) is defined. For the external cylinder containing the computational domain, a slip velocity condition is set, i.e., the derivative of the tangential velocity components and the normal velocity are set to zero ($\partial v_\theta/\partial n = 0$; $\partial v_x/\partial n = 0$; $v_n = 0$); a Neumann boundary condition for the temperature field is imposed. At the sphere surface, no-slip boundary conditions for the velocity field and constant temperature $\Theta = (T - T_{in})/(T_{sph} - T_{in}) = 1$ are prescribed.

For solving the various cases, two computational meshes are constructed (see Table 1). The mesh $m1$ with 1.7×10^6 grid points is used for the two lower Reynolds numbers $Re = 500$ and $Re = 750$, whereas for $Re = 1000$ the mesh $m2$ with 5.6×10^6 grid points is used. Details about the construction of the meshes can be seen in Fig. 1. The unstructured meshes are composed of four different zones with different grid refinements, the near wake zone ($Z1$) being the most refined one. Moreover, in the region close to the sphere, points are clustered to guarantee a good resolution in the boundary layer. In Fig. 2, the wall-normal distance to the sphere along its circumference is plotted for $Re = 750$ and $Re = 1000$. Herein, the non-dimensional wall-normal distance is defined as $y^+ = u_\tau y_n/\nu$, y_n being the wall-normal distance and u_τ the skin-friction velocity ($u_\tau = \sqrt{\tau_w/\rho}$; $\tau_w = \mu \partial u_\theta/\partial n$ is the skin friction, μ is the fluid dynamic viscosity and u_θ stands for the

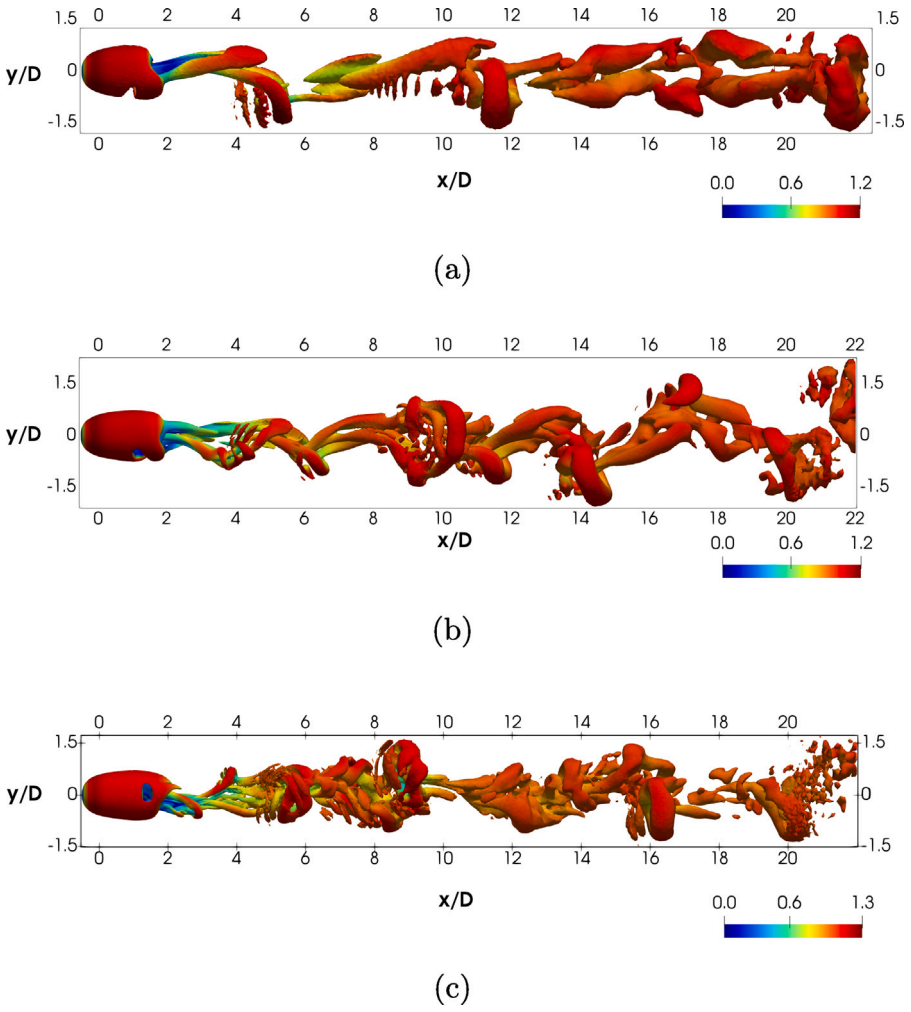

Fig. 3. Vortical structures in the wake of the sphere represented by Q-isocontours $Q = 0.01$ and coloured by the velocity magnitude. (a) $Re = 500$, (b) $Re = 750$, (c) $Re = 1000$.

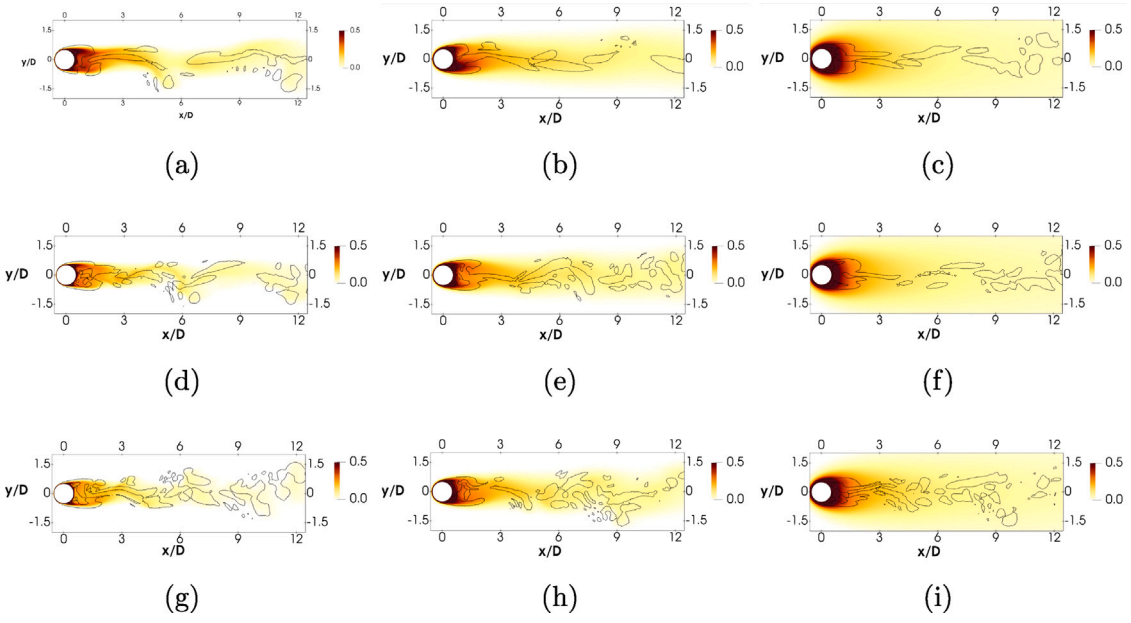

Fig. 4. Effect of the Prandtl number on the instantaneous temperature field. The temperature field is superimposed with the vortical structures identified by means of Q-isocontours (plotted in black). (a) $Re = 500$, $Pr = 0.7$; (b) $Re = 500$, $Pr = 0.1$; (c) $Re = 500$, $Pr = 0.01$; (d) $Re = 750$, $Pr = 0.7$; (e) $Re = 750$, $Pr = 0.1$; (f) $Re = 750$, $Pr = 0.01$; (g) $Re = 1000$, $Pr = 0.7$; (h) $Re = 1000$, $Pr = 0.1$; (i) $Re = 1000$, $Pr = 0.01$;.

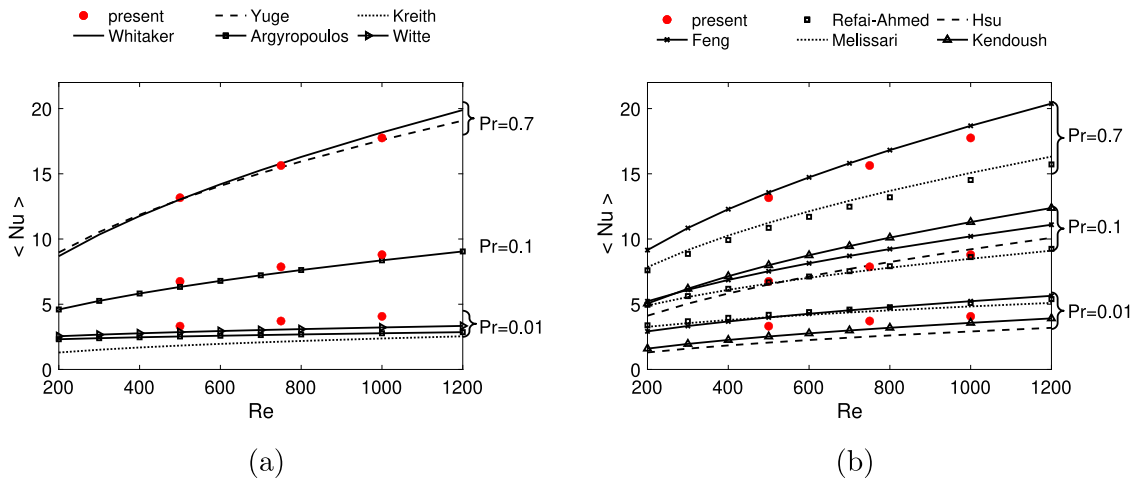

Fig. 5. Time-average Nusselt number. Comparison with results from the literature based on (a) experimental correlations, (b) theoretical correlations. See Tables 3 and 4 for information about correlations.

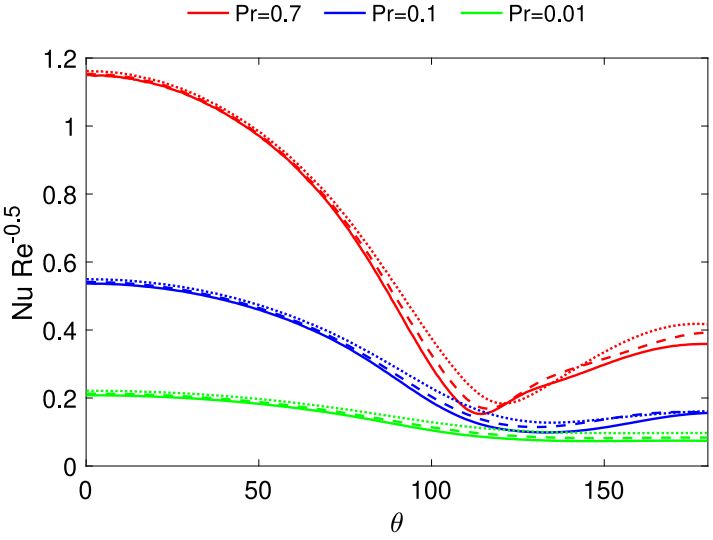

Fig. 6. Variation of local Nusselt number with Prandtl number. Solid line $Re = 1000$, dashed line $Re = 750$, dotted line $Re = 500$.

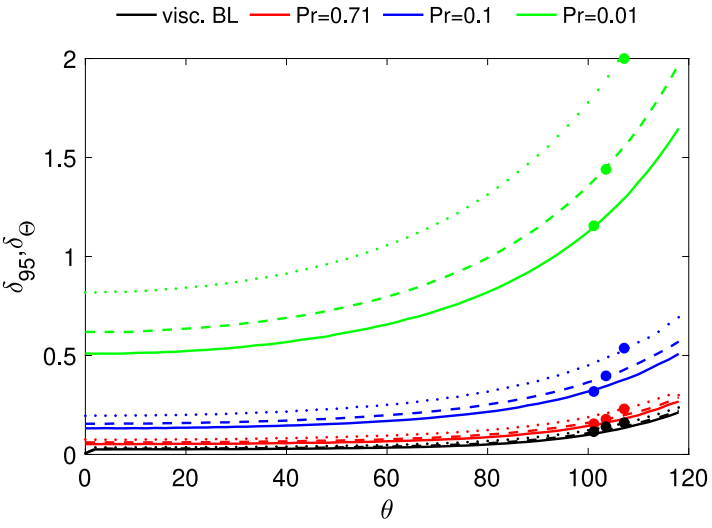

Fig. 7. Viscous and thermal boundary thicknesses for the different Reynolds and Prandtl numbers. (dotted line) $Re = 500$, (dashed line) $Re = 750$, (solid line) $Re = 1000$. The solid dots represent the location of the boundary layer separation at each Reynolds number.

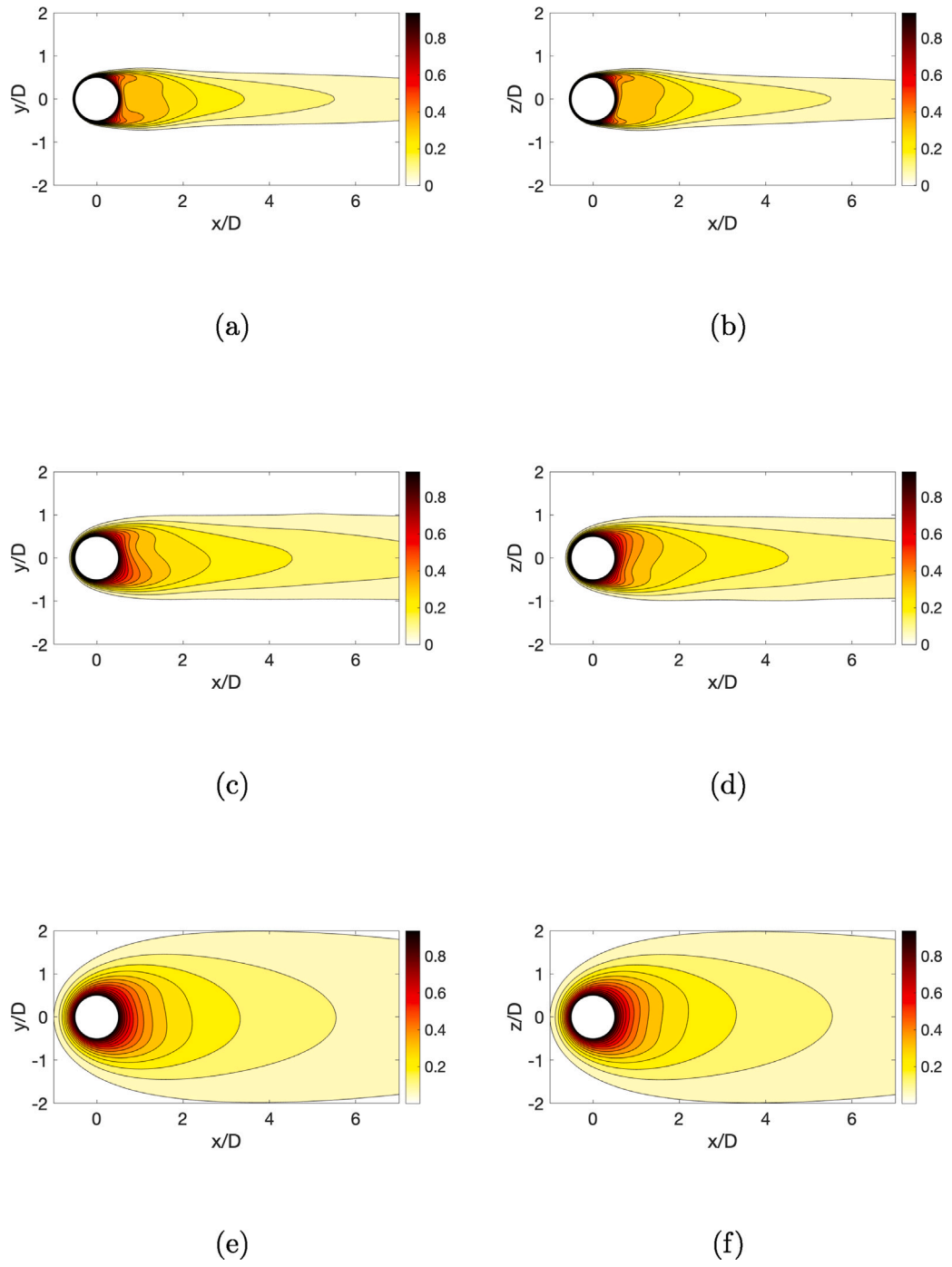

Fig. 8. Effect of the Prandtl number on the temperature distribution in the wake of the sphere at two perpendicular planes for $Re = 500$; left x–y plane, right $x - z$ plane. (a,b) $Pr = 0.7$, (c,d) $Pr = 0.1$, (e,f) $Pr = 0.01$.

Table 1
Meshes used in the simulations. N_{elem}, total number of elements, N_{gp} total number of grid points, Δ_{sph}/D size of the elements at the surface of the sphere, Δ_{z1}/D to Δ_{z4}/D size of the elements in the regions 1 to 4 in the wake of the sphere, N_{BL} number of grid points within the boundary layer at $\theta = 90°$, y^+_{max} maximum wall-normal distance (N_{BL} and y^+ are calculated for $Re = 750$ for mesh m1 and for $Re = 1000$ for mesh m2).

Mesh	N_{elem}	N_{gp}	Δ_{sph}/D	Δ_{z1}	Δ_{z2}/D	Δ_{z3}/D	Δ_{z4}/D	N_{BL}	y^+_{max}
m1	9.6×10^6	1.7×10^6	0.0050	0.050	0.08	0.12	0.75	12	0.284
m2	3.27×10^7	5.6×10^6	0.0025	0.025	0.05	0.12	0.75	15	0.336

tangential velocity at the sphere surface). As can be seen in the figure, the maximum value of the non-dimensional distance is kept below $y^+ < 1$ in all cases. These meshes were tested in Rodriguez et al. [9] and mesh m2 proved to give accurate results for both $Re = 1000$ and $Re = 10^4$. Here, it has been found that mesh m1 is accurate enough for solving the two cases at lower Reynolds numbers, i.e., $Re = 500$ and $Re = 750$. A comparison between the solution with both meshes for $Pr = 0.7$ is presented in Appendix. The collected results with mesh m1

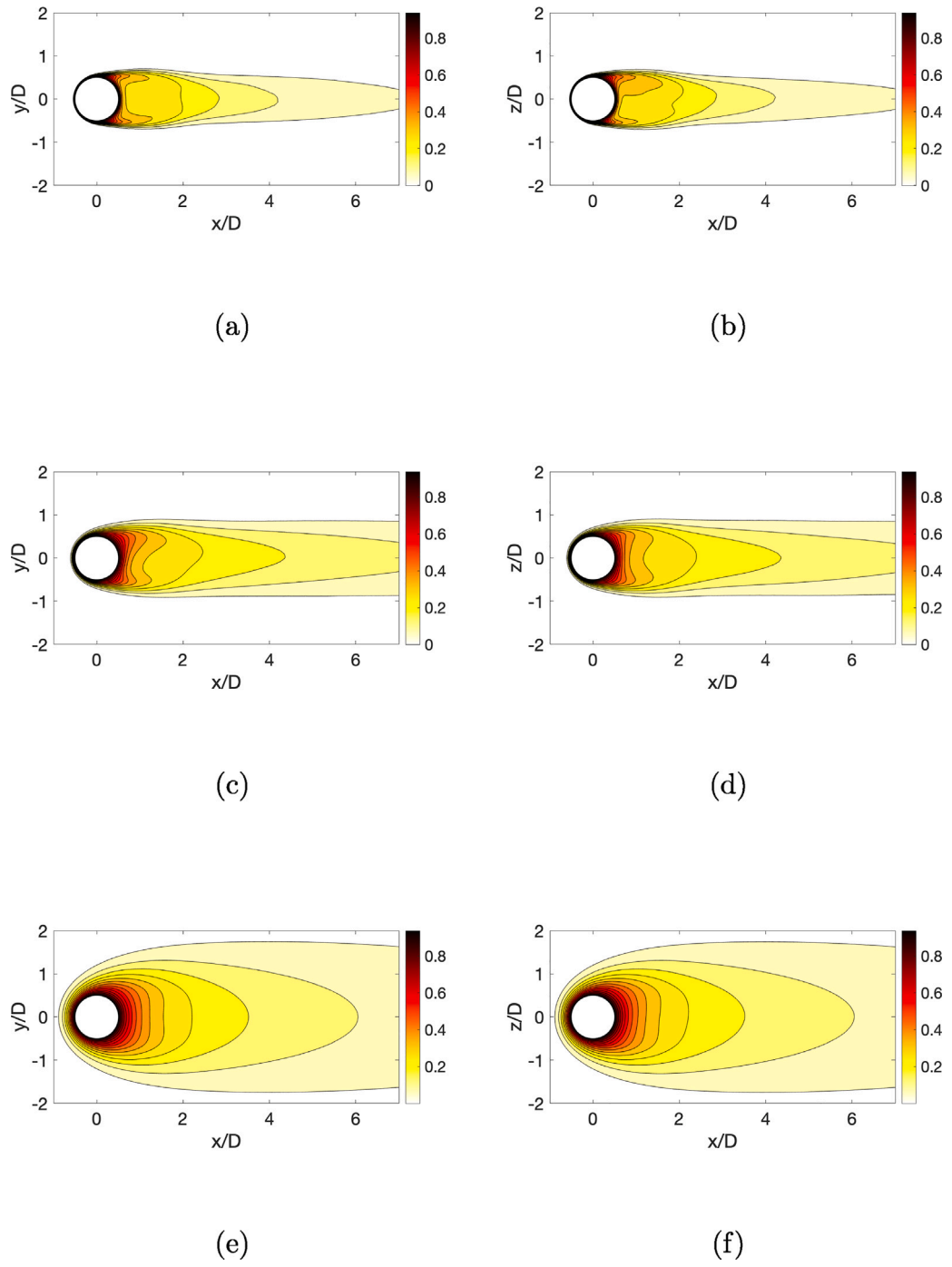

Fig. 9. Effect of the Prandtl number on the temperature distribution in the wake of the sphere at two perpendicular planes for $Re = 750$; left x–y plane, right $x - z$ plane. (a,b) $Pr = 0.7$, (c,d) $Pr = 0.1$, (e,f) $Pr = 0.01$.

have shown to be in good agreement with those obtained with mesh m2. Therefore, in order to save computational time and resources, the former mesh m1 is adopted in all computations linked to the two lower Reynolds numbers.

3. Results

This section is structured into three subsections. The first subsection discusses the differences in the instantaneous flow responsive to the Prandtl number. Owing that the temperature map is treated as a passive scalar, herein the velocity field is independent on the Prandtl number. The next two subsections deal with the time-average flow and the temperature fields concurrently. For evaluating the time-average flow, the case with $Pr = 0.7$ is advanced in time up until the statistical stationary regime is reached. In this context, the average statistics are obtained after the integration of about 250 time-units (TU, $TU = t\,U/D$). For the pair of $Pr = 0.1$ and $Pr = 0.01$, the flow is initialised with the velocity field associated with $Pr = 0.7$. Then, after the initial short transient is surpassed, the proper statistics are also integrated over the time.

3.1. Effect of the Prandtl number on the instantaneous temperature field

Coherent structures developed in the wake of the sphere for the three Reynolds numbers are depicted in Fig. 3. Vortical structures

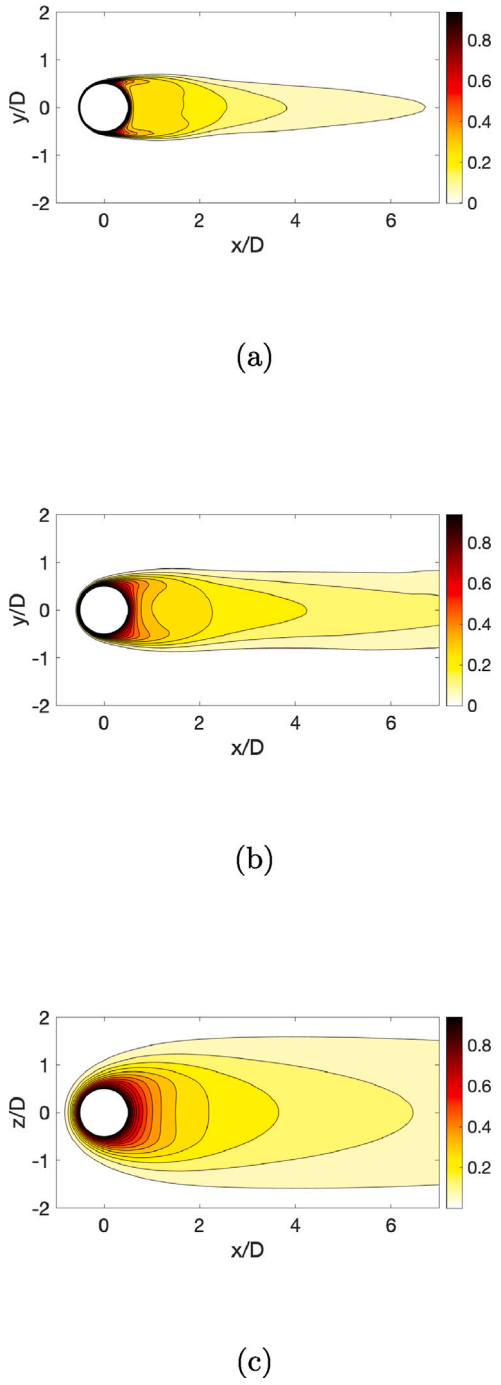

Fig. 10. Effect of the Prandtl number on the temperature distribution in the wake of the sphere for $Re = 1000$; (a) $Pr = 0.7$, (b) $Pr = 0.1$, (c) $Pr = 0.01$.

are represented using the Q-criterion proposed by Hunt et al. [45]. In the figure, Q-isocontours are coloured by the velocity magnitude. Complementing these plots, instantaneous temperature maps at the x–y plane superimposed over the vortical structures are displayed in Fig. 4. Moreover, relevant quantities, such as the average separation point, θ_s, the drag coefficient, C_D, the lift coefficient, C_L, and the recirculation length L_{rec}/D are listed in Table 2. The average separation point is defined as the angular position in the sphere where the wall shear stress attains zero. The drag coefficient is defined as the non-dimensional force on the surface in the streamwise direction $C_D = C_x = F_x/(1/2\rho U^2 A_{ref})$, whereas the lift coefficient C_L is defined in the cross-stream direction from the C_y and C_z components, i.e., $C_i = F_i/(1/2\rho U^2 A_{ref})$ with $i = 2, 3$ (or y, z). Here, the reference area A_{ref} corresponds to the cross-sectional area. The recirculation length L_{rec}/D is calculated as the average distance from the sphere in the wake centreline where the stream-wise velocity changes sign.

Table 2
Flow parameters: Drag coefficient C_D, lift coefficient C_L, separation angle θ_s and recirculation length L_{rec}/D.

Re	C_D	C_L	θ_s	L_{rec}/D
500	0.582	−0.049	106.9°	1.44
750	0.517	−0.023	103.5°	1.58
1000	0.466	-7.6×10^{-4}	101.4°	1.68

As expected, for the three Reynolds numbers under study, the flow separates laminarly from the sphere surface as shown in Fig. 3 and, the separation point moves towards the sphere apex as the Reynolds number increases (see the pertinent values summarised in Table 2). Actually, laminar separation takes place up until $Re \approx 2\times10^5$ [46] when transition to turbulence moves towards the sphere surface. Despite that there is vortex shedding at the two lower Reynolds numbers, the wake remains laminar and exhibits an asymmetric behaviour (Fig. 3a,b). In fact, at these Reynolds numbers, the mean lift coefficient C_L has a non-zero value (see Table 2), in conformity with the values reported in Refs. [47,48]. The asymmetry in the flow also affects the heat transfer as will be discussed in detail in the next subsection.

When the Reynolds number exceeds $Re = 800$, Kelvin–Helmholtz instabilities commence to show up in the separated laminar shear layer [34]. These instabilities can be observed for Reynolds number $Re = 1000$ (see Fig. 3c) as the wake experiences the transition from laminar to turbulent regime. Also, vortices are shed at random azimuthal locations in the shear layer (see discussion in Rodriguez et al. [44]). As a consequence, the average symmetry of the flow is recovered. This feature can also be deduced from the value of mean lift coefficient, which is almost zero at $Re = 1000$.

When inspecting the instantaneous temperature maps plotted in Fig. 4, it is observed that as the Prandtl number decreases compared to eddy transport the heat diffusion becomes more important, especially in the near wall region. The incremental diffusivity leads to a damping in the temperature fluctuations and the dissipation of the small scales. In fact, as can be seen in Fig. 4c,f,i, small scale temperature structures are completely attenuated at $Pr = 0.01$ and the temperature map does not follow the vortical structures of the flow. As was discussed by Grötzbach [49], due to the large thermal diffusivity of the flow at low Prandtl numbers, turbulent thermal diffusivity only becomes larger than the molecular thermal diffusivity at high Reynolds numbers (e.g., for $Pr = 0.025$ at Reynolds number $Re > 6\times10^4$). Thereby, it is expected that for the selected Reynolds numbers under study associated with $Pr = 0.01$ the heat transport is dominated solely by the thermal diffusivity of the flow.

3.2. Effect of the Prandtl number on the time-average heat transfer

The local non-dimensional heat transfer coefficient is the local Nusselt number Nu specified at the sphere surface. Nu is evaluated in terms of the local heat transfer coefficient h and the fluid thermal conductivity k as,

$$Nu = \frac{h\,D}{k} = \frac{\dot{q}}{(T_{sph} - T_{in})}\frac{D}{k} = \frac{k\partial T/\partial n}{(T_{sph} - T_{in})}\frac{D}{k} = \frac{D\partial\Theta}{\partial n} \tag{4}$$

In the above expression, $\dot{q}$ is the heat flux from the sphere, and T_{sph} and T_{in} are the temperatures at the sphere surface and at the inlet, respectively. In Fig. 5, the time average Nusselt number $\langle Nu\rangle$ is plotted against both experimental and theoretical correlations taken from the literature, which are summarised in Tables 3 and 4. In general, the plots in the figure demonstrate that the time-average Nusselt number for $Pr = 0.7$ is in good agreement with those predicted by the experimental correlations available in the literature. When Prandtl number

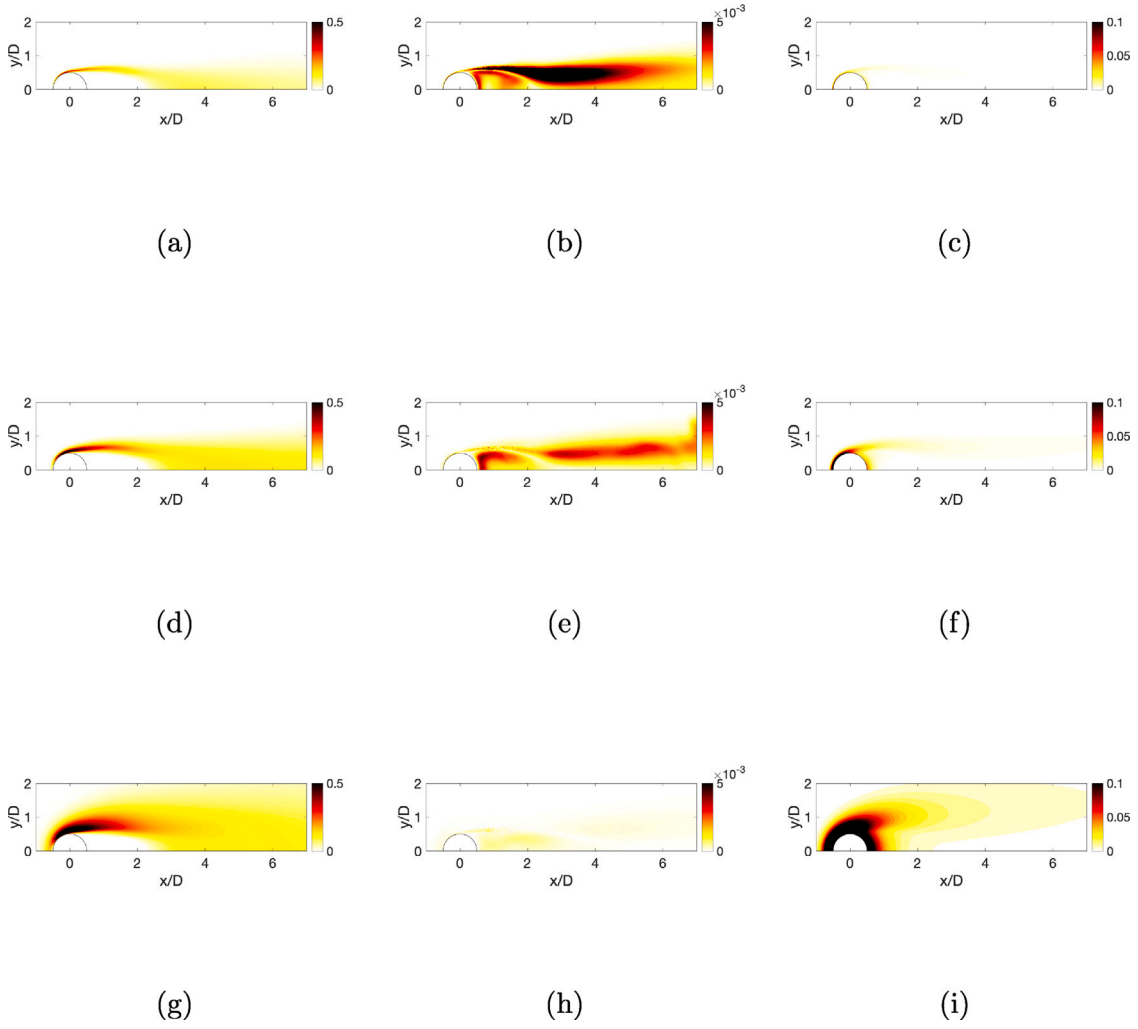

Fig. 11. Effect of the Prandtl number on the heat fluxes in the wake of the sphere for $Re = 1000$. (left) magnitude of the convective heat flux, (centre) magnitude of the turbulent heat flux, (right) magnitude of the diffusive heat flux;(a,b,c) $Pr = 0.7$, (d,e,f) $Pr = 0.1$, (g,h,i) $Pr = 0.01$.

diminishes one order of magnitude to $Pr = 0.1$ and two orders of magnitude to $Pr = 0.01$, the values of the Nusselt number are slightly larger than those predicted by the experimental correlations. However, it should be mentioned that Witte correlation [23] and Argyropoulos correlation [24] were obtained for larger Reynolds numbers than those studied here. This implies that the plot is outside the range of validity of the two experimental correlations. Moreover, the correlation by Kreith et al. [50] was obtained for rotating spheres and consequently, it is not expected to accurately work for the case under study.

A larger scattering is palpable when the computed results are plotted against the theoretical correlations. However, it should be bear in mind that some of these theoretical correlations were based on the inviscid flow hypothesis, such as those by Hsu [13] and Kendoush [16], or by using a simpler two-dimensional model, like Feng and Michaelides [27]. Nonetheless, depending on the Prandtl number, the agreement might tend to improve. In the case of the theoretical correlations based on the inviscid flow hypothesis, i.e., Kendoush correlation [16] and Hsu correlation [13], large deviations are observed at $Pr = 0.7$ (not plotted here), but their prediction improve as the Pr diminishes. This might be due to the simplistic assumption of inviscid flow, because as the Prandtl number diminishes the heat transport by diffusion gets more notoriety, especially in the separated zone behind the sphere and thus ascertain that the heat transfer estimates are more accurate at low Prandtl numbers. A different explanation can be given to the deviations observed from Melissari and Argyropoulos [25]

Table 3
Nusselt numbers based on experimental measurements.

Reference	Correlation	Observations
Yuge [17]	$2 + 0.493\ Re^{0.5}$	$10 < Re < 1800$ $Pr = 0.7$
Kreith et al. [50]	$0.178\ Re^{0.375}$	$7 \times 10^4 < Re < 10^6$ $Pr = 10^{-2}$
Witte [23]	$2 + 0.386(Re\ Pr)^{0.5}$	$3.56 \times 10^4 < Re < 1.525 \times 10^5$ $Pr = 10^{-3}$
Whitaker [22]	$2 + (0.4\ Re^{0.5} + 0.06\ Re^{2/3})Pr^{0.4}$	$3.5 < Re < 7.6 \times 10^4$ $0.71 < Pr < 380$
Argyropoulos [24]	$2 + 1.114\ Re^{0.557}\ Pr^{0.914}$	$4330 < Re < 20780$ $0.014 < Pr < 0.219$

correlation, as the model is based on global balances, which do not take into account local variations in the heat transfer coefficient. Moreover, since the model was validated for liquid metals, it most perform better at low Prandtl numbers, as can be corroborated from the comparisons.

The local time average Nusselt number Nu for the different cases is illustrated in Fig. 6. Notice that Nu has been scaled with the non-dimensional group $Nu\ Re^{-0.5}$, following the numerical model for the heat transfer in two-dimensional and rotationally symmetrical laminar boundary layer flows exposed by Frösling [20]. Complementing this figure, the influence of the Prandtl number on the viscous boundary layer thickness (δ_{95}) and the thermal boundary layer thickness (δ_Θ) for all Reynolds numbers considered is plotted in Fig. 7. Here, the viscous

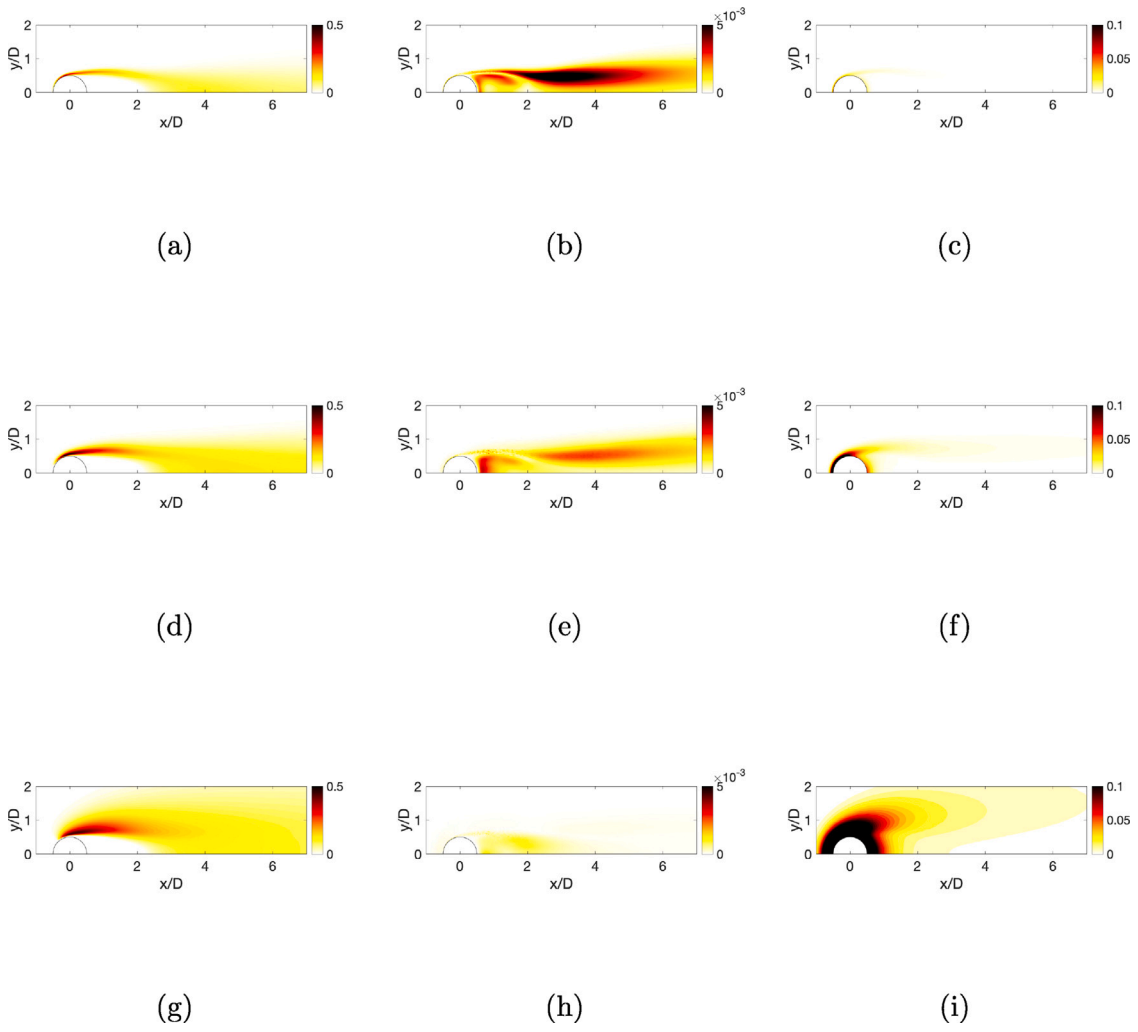

Fig. 12. Effect of the Prandtl number on the heat fluxes in the wake of the sphere for $Re = 750$. (left) magnitude of the convective heat flux, (centre) magnitude of the turbulent heat flux, (right) magnitude of the diffusive heat flux;(a,b,c) $Pr = 0.7$, (d,e,f) $Pr = 0.1$, (g,h,i) $Pr = 0.01$.

Table 4
Nusselt numbers based on numerical simulations.

Reference	Correlation	Observations
Hsu [13]	$0.921(RePr)^{0.5}$	$Re < 5 \times 10^5$ $Pr < 0.1$
Kendoush [16]	$1.13(RePr)^{1/2}$	$Re < \times 10^3$ $Pr < 0.1$
Feng and Michaelides [27]	$0.922 + (RePr)^{1/3} + 0.1Re^{2/3}Pr^{1/3}$	$Re < 2000$ $RePr < 2000$
Refai-Ahmed and Yovanovich [15]	$2 + 0.775Re^{0.5}\frac{Pr^{1/3}/\sqrt{2Re^{-0.25}+1}}{\left[1+\frac{1}{(2Re^{-0.25}+1)^3}\right]^{1/6}}$	$Re < 10^5$ $0 < Pr < \infty$
Melissari and Argyropoulos [25]	$2 + 0.47\ Re^{0.5}Pr^{0.36}$	$100 < Re < 5 \times 10^4$ $3 \times 10^{-3} < Pr < 10$

boundary layer thickness is defined as the non-dimensional distance in the wall-normal direction from the surface to the location where the tangential velocity reaches 95% of the edge velocity ($u_\theta = 0.95U_{edge}$); the edge velocity being the maximum velocity in the boundary layer in the wall normal direction. In a similar way, the thermal boundary layer thickness is defined as the location in the wall normal direction where the fluid temperature reaches 5% of the wall temperature above the free-stream temperature.

As expected, the maximum average Nusselt number is attained at the front stagnation point in the sphere and decreases gradually as the boundary layer thickens, to reach a local minima close to the location of the boundary layer separation (see also Fig. 7). For the reference case $Pr = 0.7$, although the thermal boundary layer is slightly thicker than the viscous one, both boundary layers are comparable. Moreover, as convective transport dominates, after separation occurs, the heat transfer intensifies slightly due to the incipient flow recirculation behind the sphere. When the Prandtl number decreases and the diffusive effects become more important, the thickness of the thermal boundary layer enlarges. As a result, the heat transport in the boundary layer gets dominated by the heat diffusion with the consequent reduction in the local Nusselt number.

3.3. Effect of the Prandtl number on the wake

As discussed in Section 3.1, the magnitude of the Prandtl number has a paramount influence on the temperature of the fluid in the wake behind the sphere. The average temperature fields in the wake for all the cases under study are depicted in Figs. 8–10. The size of the thermal boundary layer with the decline in the Prandtl number is readily seen in the figures. There is an important elevation in the temperature levels around the sphere, which also attenuates the heat removal from the sphere. These higher temperature levels around the sphere at low Prandtl number act as insulation with the consequent low non-dimensional heat transfer coefficient as has been discussed in the previous section.

For the particular case of $Pr = 0.7$, the temperature field follows the pathway of the velocity field. The heat transport in the vortex

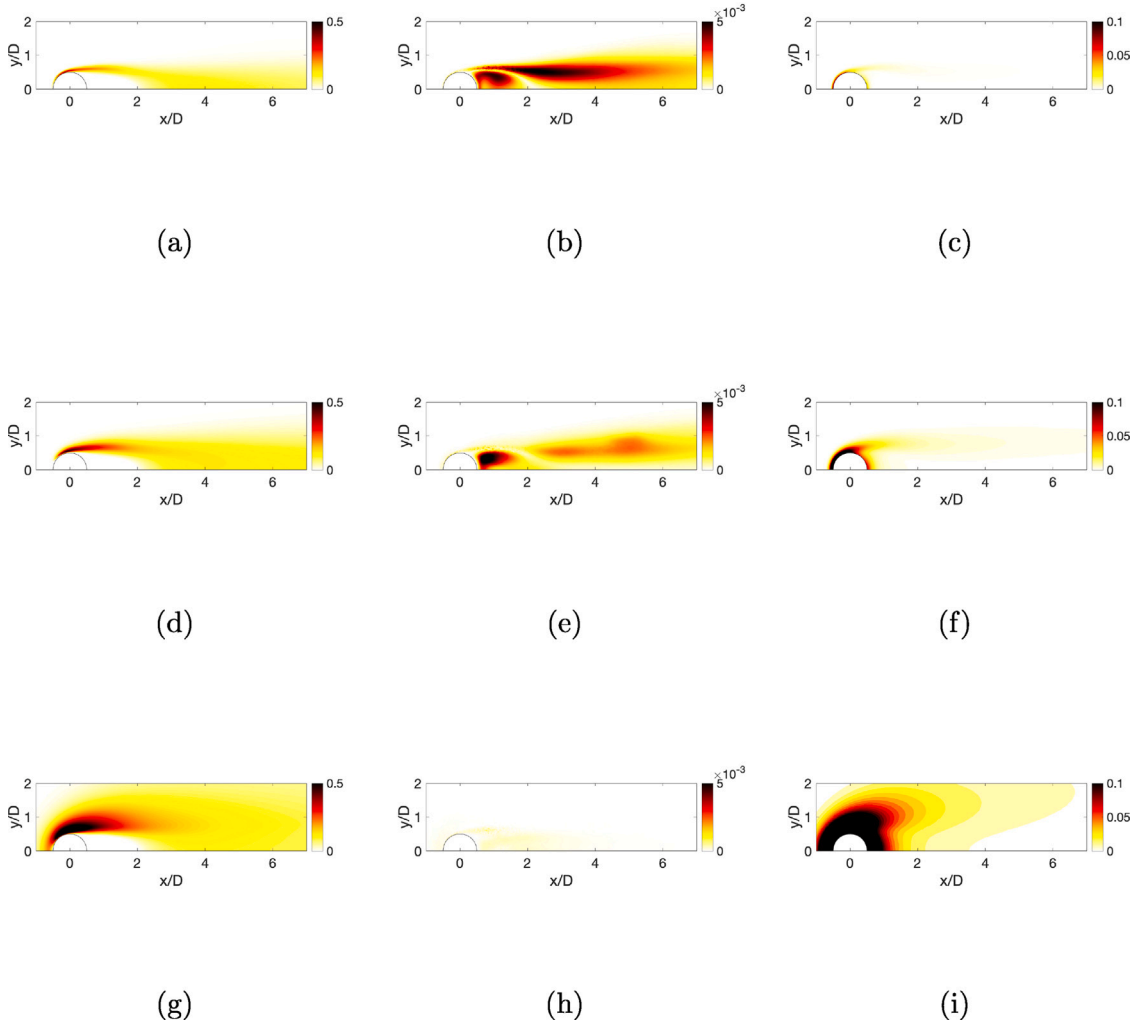

Fig. 13. Effect of the Prandtl number on the heat fluxes in the wake of the sphere for $Re = 500$. (left) magnitude of the convective heat flux, (centre) magnitude of the turbulent heat flux, (right) magnitude of the diffusive heat flux;(a,b,c) $Pr = 0.7$, (d,e,f) $Pr = 0.1$, (g,h,i) $Pr = 0.01$.

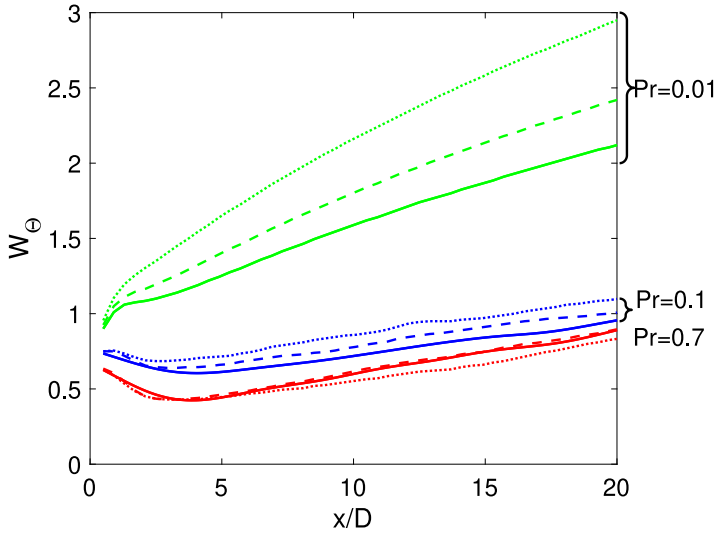

Fig. 14. Thermal wake width for the different cases. (dotted line) $Re = 500$, (dashed line) $Re = 750$, (solid line) $Re = 1000$.

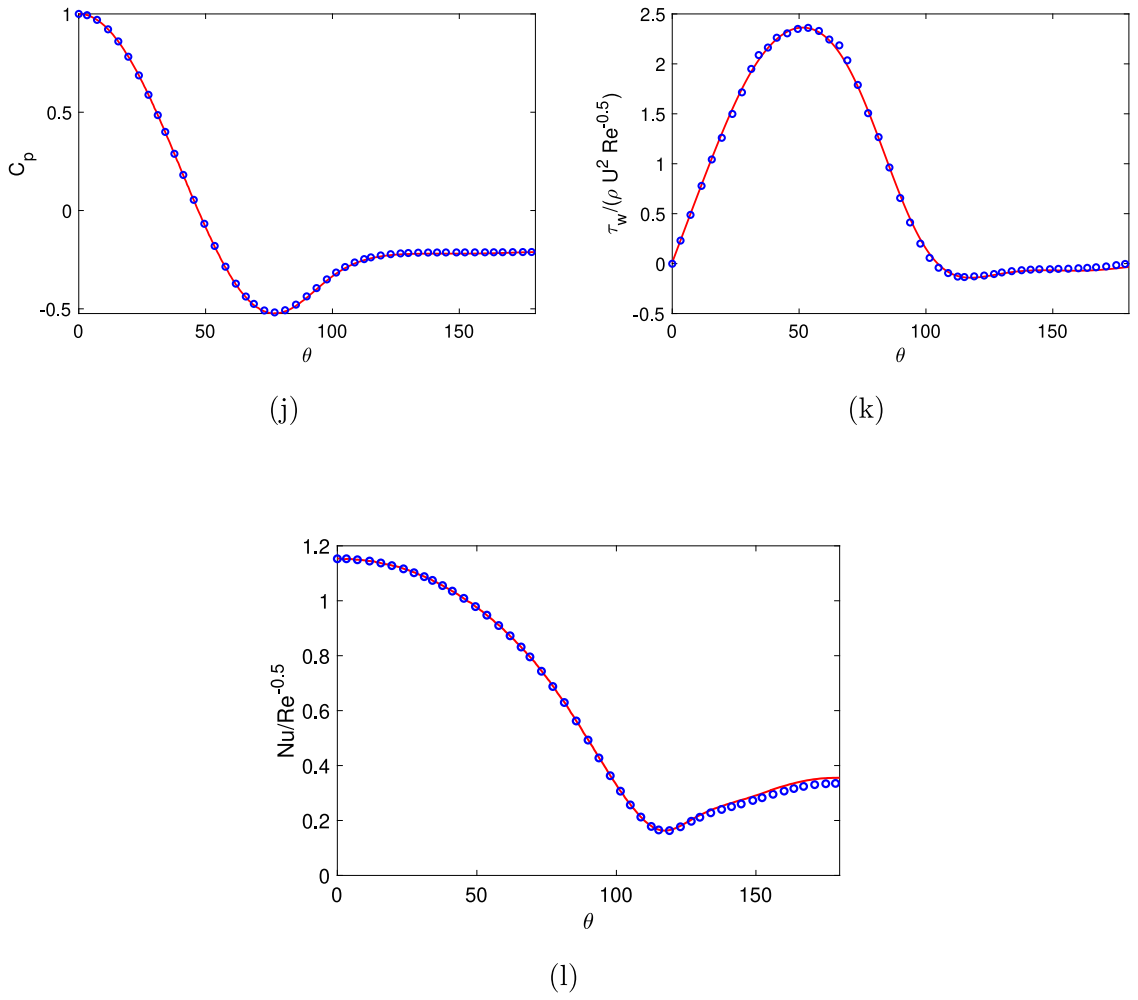

Fig. A.15. Mesh resolution studies. Comparison of the results obtained with mesh m1 and m2 at $Re = 750$, $Pr = 0.71$. (a) Pressure coefficient, (b) skin friction, (c) Nusselt number. (red line) mesh m1, (blue dots) mesh m2.

formation region is dominated by the vortex shedding process and the entrainment of colder fluid from the main stream flow. The heat from the sphere is removed by the dominant higher vorticity in the shear layer, which results in larger temperature values along it. This pattern related to the more intense transport due to the vortex shedding is attenuated as the Prandtl number diminishes, as can be seen in Figs. 8(e,f), 9(e,f) and 10c.

As commented before in Section 3.1 for the two lower Reynolds numbers, the vortex shedding process is asymmetric, which brings forth in asymmetric average temperature maps. This trend can be observed in Fig. 8 for $Re = 500$ and Fig. 9 for $Re = 750$, where the temperature maps are plotted in two perpendicular planes. At these two Reynolds numbers, the asymmetry in the vortex shedding process seems to favour a range of azimuthal locations. This behaviour ultimately influences the temperature field, especially in the vortex formation zone. The asymmetry in the vortex shedding brings forth a non-zero cross-stream force coefficient (see values of the average C_L reported in Table 2 and the discussion in Section 3.1) and as a direct consequence, an asymmetric heat transfer. The asymmetry in the heat transfer was previously reported by Bagchi et al. [48] in their numerical study of the flow and heat transfer from a sphere up to Reynolds number $Re = 500$. Nonetheless, as the flow moves downstream the vortex formation zone, the symmetry in the temperature field is gradually recovered (see Figs. 8 and 9).

An interesting feature attributable to a reduction in the Prandtl number is that the asymmetry in the vortex formation zone tends to smooth out and the symmetry is almost recovered at $Pr = 0.01$. This feature is due to an invigoration in the diffusive heat transport over the convective heat transport. When Reynolds number ascends to $Re = 1000$, the vortex shedding process occurs at random locations in the separated shear layer, as discussed in [9]. As a result, the time-averaged wake recovers its axisymmetric shape, and the temperature field becomes axisymmetric (see Fig. 10). Due to the prevalent axisymmetry in the average flow, only one plane is plotted in the figure.

Another essential issue on the temperature field is that with a reduction in the Prandtl number, the temperature decay along the wake centreline occurs at a reduced rate. This behaviour can also be understood if the viscous and turbulent heat fluxes are evaluated in the wake. The quantitative evaluation of the total heat flux (and its components) in the wake can be very useful in gaining physical insight into the heat transfer process from the heated sphere to the fluid. The total heat flux can be evaluated as

$$q_i^t = \langle u_i \Theta \rangle + \langle u_i' \Theta' \rangle - \frac{1}{Re\ Pr}\left(\frac{\partial \langle \Theta \rangle}{\partial x_i}\right) \tag{5}$$

In the above equation, $\langle \cdot \rangle$ denotes the time average fields. In Figs. 11–13, the three components of the heat flux magnitude in Eq. (5), i.e., the convective heat flux $\langle u_i \Theta \rangle$, the turbulent heat flux $\langle u_i' \Theta' \rangle$ and the diffusive part $-\frac{1}{Re\ Pr}\left(\frac{\partial \langle \Theta \rangle}{\partial x_i}\right)$ are plotted for the three Reynolds numbers under study. Analysing the figures, it can be ascertained that, qualitatively, the behaviour of the heat fluxes as a function of the Prandtl number is similar for all Reynolds numbers. As can be seen from the figures, the Prandtl number has a pronounced influence on the behaviour of the heat fluxes in the wake. On one hand, there

is an intensification of the overall heat transfer with the decline in the Prandtl number. The lower the Prandtl number, the larger the magnitude of both the diffusive and the convective heat fluxes, which further explains the lower decay ratio of the temperature along the wake centreline. On the other hand, as expected, the turbulent heat transfer diminishes with a reduction in the Prandtl number, being almost negligible at $Pr = 0.01$. Moreover, as the diffusive heat transport dominates over the turbulent heat transfer, the rate of heat transfer enlarges with cutbacks in the Prandtl number. In addition, this has a bearing on the thermal wake spread as can be observed in Figs. 8–10.

A quantitative evaluation of the thermal wake spread can be calculated from the thermal half-wake width, which is shown in Fig. 14. The thermal half-wake width has been defined as in Legendre et al. [51], as the distance where the non-dimensional temperature $\Theta(x/D, r/D)$ reaches a magnitude equal to $e^{-1/2}$ the value at the wake centreline, i.e., $\Theta(x/D, r/D) = \Theta(x/D, 0)e^{-1/2}$. It is important to point out that for computing the average wake width, the temperature profiles have been averaged in the azimuthal direction, so that asymmetries in the flow have not been taken into account. As can be readily seen from Fig. 14, whenever $Pr = 0.7$, the wake width is almost invariant with the Reynolds number. However, for lower Prandtl numbers, the wake width increases and subtle differences connected to the Reynolds number are manifested. This feature indeed signifies that the intensification in the heat transfer due to diffusive transport becomes more relevant with decrements in the Prandtl number. Specifically, when the Prandtl number descends from $Pr = 0.7$ to $Pr = 0.01$ (about two orders of magnitude), the heat transfer augmentation can reach 2.3 to 3.5 times at $x/D = 20$ when the Reynolds number shrinks from $Re = 1000$ to $Re = 500$.

4. Conclusions

In the present study, direct numerical simulations of certain fluid flows around a sphere at Reynolds numbers of $Re = 500$, 750 and 1000 have been performed to examine the susceptibility of the Prandtl number on the sphere and wake ensemble. The Prandtl numbers selected are $Pr = 0.01$, 0.1 and 0.7.

As the Prandtl number decreases from $Pr = 0.7$, the heat diffusion becomes dominant over the eddy transport, which leads to a damping in the temperature and heat fluxes fluctuations at all Reynolds numbers. For the two lower Reynolds numbers $Re = 500$ and $Re = 750$, the wake turns asymmetric, which results in a non-zero cross-stream force coefficient. This asymmetry in the flow has a repercussion on the heat transfer, the near wake temperature and the heat fluxes. Such asymmetry tends to disappear as the heat transport by diffusion dominates over the turbulent heat transport with gradual decays in the Prandtl number. Moreover, irrespective of the Reynolds number, the thermal wake spread enlarges about 2.3 to 3.5 times at $x/D = 20$ with Pr decrements from 0.7 to 0.01.

As expected, the Prandtl number plays a preponderant role on the local and average heat transfer coefficients. As the Prandtl number decreases, coupled with the dominance of the diffusion heat transport, the boundary layer thickens with the consequent reduction in the local and average Nusselt number. The average Nusselt numbers computed in the present study are in fair agreement with experimental-based correlations reported previously in the literature. When compared with theoretical models, a larger scattering for Prandtl number $Pr = 0.7$ has been observed. However, this observation has been attributed to the separation of the flow that occurs in the rear side of the sphere. This aspect is neglected when the inviscid flow hypothesis is invoked in the theoretical models.

Declaration of competing interest

The authors declare that they have no known competing financial interests or personal relationships that could have appeared to influence the work reported in this paper.

Data availability

Data will be made available on request.

Acknowledgements

This work has been partially financially supported by the Ministerio de Ciencia e Innovación, Spain (Ref. PID2020-116937RB-C22). We also acknowledge Red Española de Supercomputación (RES) for awarding us access to the MareNostrum IV machine based in Barcelona, Spain (Ref. IM-2020-2-0013).

Appendix. Grid resolution studies

In order to corroborate that mesh m1 (see Table 1) used for solving the cases dealing with $Re = 500$ and $Re = 750$ has credible accuracy, simulations for combinations of $Re = 750$ and $Pr = 0.7$ have been also performed with mesh m2. The comparison of the pressure distribution, skin friction and Nusselt number along the sphere circumference is plotted in Fig. A.15. As can be seen from the figure, the results resting on mesh m1 manifest in good agreement with those obtained with the high-resolution mesh m2 for all quantities analysed.

References

[1] S.C.R. Dennis, J.D.A. Walker, J.D. Hudson, Heat transfer from a sphere at low Reynolds numbers, J. Fluid Mech. 60 (2) (1973) 273–283, http://dx.doi.org/10.1017/S0022112073000169.

[2] A. Yamanaka, N.M.I. T. Yuki, Combined forced and natural convective heat transfer from spheres at small Reynolds number, J. Chem. Eng. Jpn. 9 (6) (1976) 445–449, http://dx.doi.org/10.1252/jcej.9.445.

[3] T. Chen, A. Mucoglu, Analysis of mixed forced and free convection about a sphere, Int. J. Heat Mass Transfer 20 (8) (1977) 867–875, http://dx.doi.org/10.1016/0017-9310(77)90116-8, URL https://www.sciencedirect.com/science/article/pii/0017931077901168.

[4] B.A. Finlayson, J.W. Olson, Heat transfer to spheres at low to intermediate reynolds numbers, Chem. Eng. Commun. 58 (1–6) (1987) 431–447, http://dx.doi.org/10.1080/00986448708911980.

[5] H. Zhao, X. Liu, D. Li, A. Wei, K. Luo, J. Fan, Vortex dynamics of a sphere wake in proximity to a wall, Int. J. Multiph. Flow. 79 (2016) 88–106, http://dx.doi.org/10.1016/j.ijmultiphaseflow.2015.10.005.

[6] J.B. Will, N.P. Kruyt, C.H. Venner, An experimental study of forced convective heat transfer from smooth, solid spheres, Int. J. Heat Mass Transfer 109 (2017) 1059–1067, http://dx.doi.org/10.1016/j.ijheatmasstransfer.2017.02.018.

[7] R. van Hout, J. Eisma, G.E. Elsinga, J. Westerweel, Experimental study of the flow in the wake of a stationary sphere immersed in a turbulent boundary layer, Phys. Rev. Fluids 3 (2) (2018) 024601, http://dx.doi.org/10.1103/PhysRevFluids.3.024601.

[8] B. Hema Sundar Raju, D. Nath, S. Pati, Effect of Prandtl number on thermo-fluidic transport characteristics for mixed convection past a sphere, Int. Commun. Heat Mass Transfer 98 (2018) 191–199, http://dx.doi.org/10.1016/j.icheatmasstransfer.2018.08.013.

[9] I. Rodriguez, O. Lehmkuhl, M. Soria, S. Gomez, M. Domınguez-Pumar, L. Kowalski, Fluid dynamics and heat transfer in the wake of a sphere, Int. J. Heat Fluid Flow 76 (2019) 141–153.

[10] B.H.S. Raju, D. Nath, S. Pati, Analysis of mixed convective heat transfer past an isoflux/isothermal sphere: Influence of Prandtl number, Phys. Scr. 95 (8) (2020) 85211, http://dx.doi.org/10.1088/1402-4896/ab9f7c.

[11] F. Giacobbe, Heat transfer capability of selected binary gaseous mixtures relative to helium and hydrogen, Appl. Therm. Eng. 18 (3) (1998) 199–206, http://dx.doi.org/10.1016/S1359-4311(97)00019-7.

[12] A. Campo, M.M. Papari, E. Abu-Nada, Estimation of the minimum Prandtl number for binary gas mixtures formed with light helium and certain heavier gases: Application to thermoacoustic refrigerators, Appl. Therm. Eng. 31 (16) (2011) 3142–3146, http://dx.doi.org/10.1016/j.applthermaleng.2011.05.002.

[13] C.J. Hsu, Heat transfer to liquid metals flowing past spheres and elliptical-rod bundles, Int. J. Heat Mass Transfer 8 (2) (1965) 303–315, http://dx.doi.org/10.1016/0017-9310(65)90118-3.

[14] S. Sideman, The equivalence of the penetration and potential flow theories, Ind. Eng. Chem. Res. 58 (2) (1966) 54–58.

[15] G. Refai Ahmed, M.M. Yovanovich, Approximate analytical solution of forced convection heat transfer from isothermal spheres for all Prandtl numbers, J. Heat Transfer 116 (4) (1994) 838–843, http://dx.doi.org/10.1115/1.2911456.

[16] A.A. Kendoush, Low Prandtl number heat transfer to fluids flowing past an isothermal spherical particle, Int. J. Heat Fluid Flow 16 (4) (1995) 291–297, http://dx.doi.org/10.1016/0142-727X(95)00025-L.
[17] T. Yuge, Experiments on heat transfer from spheres including combined natural and forced convection, J. Heat Transfer 82 (3) (1960) 214–220, http://dx.doi.org/10.1115/1.3679912.
[18] G.D. Raithby, E.R.G. Eckert, The effect of turbulence parameters and support position on the heat transfer from spheres, Int. J. Heat Mass Transfer 11 (1968) 1233–1252.
[19] G.J. Kowalski, J.W. Mitchell, Heat transfer from spheres in the naturally turbulent, outdoor environment, J. Heat Transf. 98 (4) (1976) 649–653, http://dx.doi.org/10.1115/1.3450614.
[20] N. Frossling, Uber die Verdunstung fallender Tropfen (The evaporation of falling drops), Gerlands Beitrage Zur Geophysik 52 (1938) 107–216.
[21] G.C. Vliet, G. Leppert, Forced convection heat transfer from an isothermal sphere to water, J. Heat Transfer 83 (1961) 163, http://dx.doi.org/10.1115/1.3680504.
[22] S. Whitaker, Forced convection heat transfer correlations for flow in pipes, past flat plates, single cylinders, single spheres, and for flow in packed beds and tube bundles, AIChE J. 18 (2) (1972) 361–371, http://dx.doi.org/10.1002/aic.690180219.
[23] L.C. Witte, An experimental study of forced-convection heat transfer from a sphere to liquid sodium, J. Heat Transfer 90 (1) (1968) 9–12, http://dx.doi.org/10.1115/1.3597469.
[24] S.A. Argyropoulos, A.C. Mikrovas, An experimental investigation on natural and forced convection in liquid metals, Int. J. Heat Mass Transfer 39 (3) (1996) 547–561, http://dx.doi.org/10.1016/0017-9310(95)00138-Y.
[25] B. Melissari, S.A. Argyropoulos, The identification of transition convective regimes in liquid metals using a computational approach, Prog. Comput. Fluid Dyn. 4 (2) (2004) 69–77, http://dx.doi.org/10.1504/PCFD.2004.003792.
[26] Z.G. Feng, E.E. Michaelides, Unsteady heat transfer from a sphere at small Peclet numbers, J. Fluids Eng. 118 (1) (1996) 96–102, http://dx.doi.org/10.1115/1.2817522.
[27] Z.-G. Feng, E.E. Michaelides, A numerical study on the transient heat transfer from a sphere at high Reynolds and peclet numbers, Int. J. Heat Mass Transfer 43 (2) (2000) 219–229, http://dx.doi.org/10.1016/S0017-9310(99)00133-7.
[28] S.D. Dhole, R.P. Chhabra, V. Eswaran, A numerical study on the forced convection heat transfer from an isothermal and isoflux sphere in the steady symmetric flow regime, Int. J. Heat Mass Transfer 49 (5–6) (2006) 984–994, http://dx.doi.org/10.1016/j.ijheatmasstransfer.2005.09.010.
[29] S. Ganguli, S.K. Lele, Drag of a heated sphere at low Reynolds numbers in the absence of buoyancy, J. Fluid Mech. 869 (2019) 264–291, http://dx.doi.org/10.1017/jfm.2019.187.
[30] D. Nath, B. Raju, Effect of isoflux thermal boundary condition on mixed convective heat transfer from a sphere for liquid metals, Int. J. Ambient Energy (2019) 1–19, http://dx.doi.org/10.1080/01430750.2019.1636881.
[31] I. Rodriguez, O. Lehmkuhl, M. Soria, On the effects of the free-stream turbulence on the heat transfer from a sphere, Int. J. Heat Mass Transfer 164 (2021) 120579, http://dx.doi.org/10.1016/j.ijheatmasstransfer.2020.120579.
[32] A. Campo, S. Chikh, M.M. Papari, M.R. Mobinipouya, Superior convective heat transport for laminar boundary layer flow over a flat plate using binary gas mixtures with light helium and selected heavier gases, J. Heat Transfer (5) (2010) http://dx.doi.org/10.1115/1.4000433.
[33] T. Iida, R.I.L. Guthrie, The Thermophysical Properties of Metallic Liquids: Volume 1 — Fundamentals, Oxford Scholarship Online, 2015.
[34] H. Sakamoto, H. Haniu, The formation mechanism and shedding frequency of vortices from a sphere in uniform shear flow, J. Fluid Mech. 287 (1995) 151–171.
[35] A. Tomboulides, S. Orszag, Numerical investigation of transitional and weak turbulent flow past a sphere, J. Fluids Mech. 416 (2000) 45–73.
[36] M. Vázquez, G. Houzeaux, S. Koric, A. Artigues, J. Aguado-Sierra, R. Arís, D. Mira, H. Calmet, F. Cucchietti, H. Owen, A. Taha, E.D. Burness, J.M. Cela, M. Valero, Alya: Multiphysics engineering simulation toward exascale, J. Comput. Sci. 14 (2016) 15–27, http://dx.doi.org/10.1016/j.jocs.2015.12.007.
[37] O. Lehmkuhl, G. Houzeaux, H. Owen, G. Chrysokentis, I. Rodriguez, A low-dissipation finite element scheme for scale resolving simulations of turbulent flows, J. Comput. Phys. 390 (2019) 51–65.
[38] F. Capuano, G. Coppola, L. Rández, L. de Luca, Explicit Runge–Kutta schemes for incompressible flow with improved energy-conservation properties, J. Comput. Phys. 328 (2017) 86–94.
[39] F.X. Trias, O. Lehmkuhl, A self-adaptive strategy for the time integration of Navier–Stokes equations, Numer. Heat Transf. B 60 (2) (2011) 116–134, http://dx.doi.org/10.1080/10407790.2011.594398.
[40] I. Rodriguez, O. Lehmkuhl, On the characteristics of the super-critical wake behind a circular cylinder, Fluids 6 (11) (2021) 396, http://dx.doi.org/10.3390/fluids6110396, URL https://www.mdpi.com/2311-5521/6/11/396.
[41] D. Pastrana, J.C. Cajas, O. Lehmkuhl, I. Rodríguez, G. Houzeaux, Large-eddy simulations of the vortex-induced vibration of a low mass ratio two-degree-of-freedom circular cylinder at subcritical Reynolds numbers, Comput. Fluids 173 (2018) 118–132.
[42] A. Miró, M. Soria, J.C. Cajas, I. Rodríguez, Numerical study of heat transfer from a synthetic impinging jet with a detailed model of the actuator membrane, Int. J. Therm. Sci. 136 (2019) 287–298, http://dx.doi.org/10.1016/j.ijthermalsci.2018.10.017.
[43] I. Rodriguez, O. Lehmkuhl, R. Borrell, Effects of the actuation on the boundary layer of an airfoil at Reynolds number $Re = 60000$, Flow Turbul. Combust. 390 (2020) 51–65, http://dx.doi.org/10.1007/s10494-020-00160-y.
[44] I. Rodríguez, R. Borrell, O. Lehmkuhl, C.D. Pérez-Segarra, A. Oliva, Direct numerical simulation of the flow over a sphere at Re=3700, J. Fluid Mech. 679 (2011) 263–287, http://dx.doi.org/10.1017/jfm.2011.136.
[45] J. Hunt, A. Wray, P. Moin, Eddies, Stream and Convergence Zones in Turbulent Flows, Tech. Rep. CTR-S88, Center for Turbulent Research, Stanford University, Palo Alto, CA, USA, 1988.
[46] E. Achenbach, Experiments on the flow past spheres at very high Reynolds numbers, J. Fluid Mech. 54 (1972) 565–575.
[47] T.A. Johnson, V.C. Patel, Flow past a sphere up to a Reynolds number of 300, J. Fluid Mech. 378 (1999) 19–70.
[48] P. Bagchi, M. Ha, S. Balachandar, Direct numerical simulation of flow and heat transfer from a sphere in a uniform cross-flow, J. Fluids Eng. 123 (2001) 347–358.
[49] G. Grötzbach, Challenges in low-Prandtl number heat transfer simulation and modelling, Nucl. Eng. Des. 264 (2013) 41–55, http://dx.doi.org/10.1016/j.nucengdes.2012.09.039.
[50] F. Kreith, L. Roberts, J. Sullivan, S. Sinha, Convection heat transfer and flow phenomena of rotating spheres, Int. J. Heat Mass Transfer 6 (1963) 881–895.
[51] D. Legendre, A. Merle, J. Magnaudet, Wake of a spherical bubble or a solid sphere set fixed in a turbulent environment, Phys. Fluids 18 (4) (2006) 1–5, http://dx.doi.org/10.1063/1.2191885.